Biogeosciences Discuss., 3, 803–836, 2006
www.biogeosciences-discuss.net/3/803/2006/


**Biogeosciences Discussions**

*Biogeosciences Discussions* is the access reviewed discussion forum of *Biogeosciences*

# Reconciling surface ocean productivity, export fluxes and sediment composition in a global biogeochemical ocean model

**M. Gehlen[1], L. Bopp[1], N. Emprin[1], O. Aumont[2], C. Heinze[3], and O. Ragueneau[4]**

[1]Laboratoire des Sciences du Climat et de l'Environnement (LSCE/IPSL), Orme des Merisiers, Bât. 712, CEA/Saclay, 91198 Gif-sur-Yvette Cedex, France
[2]LOCEAN/IPSL, Centre IRD de Bretagne, BP 70, 29280 Plouzané, France
[3]University of Bergen, Geophysical Institute & Bjerkness Centre for Climate Research, Allegaten 70, N-5007 Bergen Bergen, Norway
[4]Institut Universitaire Européen de la Mer, Place Copernic, Technopôle Brest-Iroise, 29280 Plouzané, France

Received: 24 April 2006 – Accepted: 17 May 2006 – Published: 28 June 2006

Correspondence to: M. Gehlen (marion.gehlen@cea.fr)



**Abstract**

This study focuses on an improved representation of the biological soft tissue pump in the global three-dimensional biogeochemical ocean model PISCES. We compare three parameterizations of particle dynamics: (1) the model standard version including two particle size classes, aggregation-disaggregation and prescribed sinking speed; (2) an aggregation-disaggregation model with a particle size spectrum and prognostic sinking speed; (3) a mineral ballast parameterization with no size classes, but prognostic sinking speed. In addition, the model includes a description of surface sediments and organic carbon early diagenesis. The integrated representation of material fluxes from the productive surface ocean down to the sediment-water interface allows taking advantage of surface ocean observations, sediment trap data and exchange fluxes at the sediment-water interface. The capability of the model to reproduce yearly averaged particulate organic carbon fluxes and benthic oxygen demand does at first order not dependent on the resolution of the particle size spectrum. Model results obtained with the standard version and with the one including a particle size spectrum and prognostic sinking speed are not significantly different. Both model versions overestimate particulate organic carbon between 1000 and 2000 m, while deep fluxes are of the correct order of magnitude. Predicted benthic oxygen fluxes correspond with respect to their large scale distribution and magnitude to data based estimates. Modeled particulate organic C fluxes across the mesopelagos are most sensitive to the intensity of zooplankton flux feeding. An increase of the intensity of flux feeding in the standard version results in lower mid- and deep-water particulate organic carbon fluxes, shifting model results to an underestimation of particulate organic carbon fluxes in the deep. The corresponding benthic oxygen fluxes are too low. The model version including the mineral ballast parameterization yields an improved fit between modeled and observed particulate organic carbon fluxes below 2000 m and down to the sediment-water interface. Our results suggest that aggregate formation alone might not be sufficient to drive an intense biological pump. The later is most likely driven by the combined effect of

aggregate formation and mineral ballasting.

## 1 Introduction

There are two pathways for the drawdown of carbon from the surface ocean and its removal from the ocean reservoir: the production of particulate organic carbon (POC) during photosynthesis and the formation of carbonate shells (PIC) during biomineralization, followed by the sinking of these particles out of surface ocean waters and their incorporation to surface sediments. Both pathways affect the surface ocean carbonate system and thus air-sea exchanges of $CO_2$ in contrasting ways. During photosynthesis dissolved inorganic carbon (DIC) is consumed together with nutrients to form POC thereby decreasing the $pCO_2$ of surface ocean waters. The resulting DIC deficit is filled by $CO_2$ released by respiration of POC either in surface waters or mixed up from deeper layers and exchanged with the atmosphere. The time scales at which C bound into POC is subtracted to air-sea exchange depends on its depth of remineralization. Conceptually, time scales range from days for shallow remineralization in well mixed waters to geological time scales for the fraction buried in marine sediments. The production and export of POC is referred to as "the biological pump" (Volk and Hoffert, 1985). The precipitation of PIC as hard parts of carbonate shells increases the $pCO_2$ of surface waters (carbonate counter-pump). Particulate inorganic C penetrates deeper in the water columun compared to POC. Its dissolution releases alkalinity which in turn titrates part of the $CO_2$ released during POC respiration. Moreover, recent studies suggest that PIC is the main carrier phase of POC to the deep ocean (Armstrong et al., 2002; Francois et al., 2002; Klaas and Archer, 2002).

The past decade has witnessed the rapid development of global ocean biogeochemical models. The growing awareness of the role of biology in the shaping of biogeochemical fluxes and its potential evolution in response to global climate change is at the origin of increasingly complex descriptions of the surface ocean ecosystem up to the first level of consumers. State-of-the-art models (Aumont and Bopp, 2005; Le Quéré



et al., 2005; Moore et al., 2004) now distinguish between different plankton functional types (silicifiers, N-fixing plankton, calcifiers, zooplankton of different size-classes) and co-limitation by macro- and micronutrients (Fe). Despite these advances, the fate of export production is still mostly described in a rather simplified way by imposing empirical functions (e.g. Suess, 1980; Betzer et al., 1984; Martin et al., 1987; Armstrong et al., 2002) to describe the distribution of particulate matter across the water column.

While export fluxes are differentiated by their chemical composition (e.g. POC, PIC and biogenic opal), marine particles are of diverse origin and composition. They range from individual plankton cells or fecal pellets to complex aggregates made of different types of primary particles trapped in a mucilaginous matrix. Fluxes of marine particles display strong regional and temporal variability in response to production regimes and their seasonality. There is growing evidence that upper ocean ecosystems contrasting in terms of primary productivity, f-ratio, seasonality etc. are characterized by quite different efficiencies in terms of C transfer to the meso- and bathypelagos. These relationships need to be taken into account in order to correctly assess effects of future changes in ecosystem structure and export fluxes on atmospheric $CO_2$ exchange, as well as to quantify the potential of artificial Fe fertilization as a sink for $CO_2$.

In this paper, we compare and evaluate three different schemes of particle flux parameterizations for their use in biogeochemical global circulation models: The PISCES standard version (two size classes, aggregation-disaggregation, prescribed sinking speed), an aggregation-disaggregation model (particle size spectrum, prognostic sinking speed), a mineral ballast parameterization (no size classes, prognostic sinking speed). We aim at an integrated representation of material fluxes from the productive surface ocean down to the sediment-water interface. This enables to take advantage of the variety of observations available for model output–data comparison.

## 2 Model description

### 2.1 The biogeochemical global ocean model

The biogeochemical model PISCES (Aumont et al., 2003; Aumont and Bopp, 2006) is based on HAMOCC5 (Aumont et al., 2003). It simulates the biogeochemical cycle of oxygen, carbon and of the main nutrients controlling marine phytoplankton growth: nitrate and ammonium, phosphate, silicate and iron. The nutrient concentration is linked through a constant Redfield ratio and phytoplankton growth is limited by the external availability of nutrients. The cycles of carbon and nitrogen are decoupled in the model to a certain degree by nitrogen fixation and denitrification.

The model distinguishes two phytoplankton size-classes corresponding to nanophytoplankton and diatoms, and two zooplankton size classes which are microzooplankton and mesozooplankton. For all species, the C/N/P ratios are assumed constant. The prognostic variables of phytoplankton are total biomass, iron, chlorophyll and silicon contents. The internal ratios of Fe/C, Chl/C and Si/C of phytoplankton are predicted by the model. For zooplankton, the total biomass is the only prognostic variable. The bacterial pool is not modeled explicitly.

The model distinguishes three non-living compartments: semi-labile dissolved organic carbon (DOC) with timescales of several weeks to several years, two size classes of particulate organic carbon (small particles = $POC_s$ and big particles = $POC_b$). While the C/N/P composition of dissolved and particulate matter is tied to Redfield stochiometry, the iron, silicon and carbonate contents of the particles are diagnosed.

A detailed description of PISCES, including model equations and parameters is available as supplementary material in Aumont and Bopp (2006). In addition to the ecosystem description, PISCES simulates dissolved inorganic carbon and total alkalinity (carbonate alkalinity + borate + water). The carbon chemistry is computed following the OCMIP protocols (http://www.ipsl.jussieu.fr/OCMIP).



### 2.2 Particle flux parameterizations

We limit the presentation of model parameterizations to processes interfering with the fate of particulate matter (POC, biogenic silica or BSi, and carbonate) in the water column.

#### 2.2.1 Standard version: two particle size classes, prescribed sinking speed

The two particulate detrital pools ($POC_s$ and $POC_b$) are fueled by mortality, loss through aggregation from nanophytoplankton and diatoms, fecal pellet production, grazing and aggregation. Mineralization of particulate organic carbon together with excretion contributes to the semi-labile pool of dissolved organic carbon. Differential settling and turbulence promote particle aggregation ($\phi$). Aggregation transfers carbon from the semi-labile DOC pool to the small particles ($\phi_{\text{agg}}^{DOC\rightarrow POCs}$) and to the big particles ($\phi_{\text{agg}}^{DOC\rightarrow POCb}$). Similarly, the compartments of small and big particles are linked by aggregation ($\phi_{\text{agg}}^{POCs\rightarrow POCb}$). The aggregation terms are described by :

$$\begin{aligned}
\phi_{\text{agg}}^{DOC\rightarrow POCs} &= \phi_1^{DOC}\,\text{sh}\cdot DOC^2 + \phi_2^{DOC}\,sh\cdot DOC\cdot POC_s \\
\phi_{\text{agg}}^{DOC\rightarrow POCb} &= \phi_3^{DOC}\,sh\cdot DOC\cdot POC_b \\
\phi_{\text{agg}}^{POCs\rightarrow POCb} &= \phi_1^{POCs}\,sh\cdot POC_s^2 + \phi_2^{POCs}\,sh\cdot POC_b\cdot POC_s + \phi_3^{POCs}\,POC_s^2 + \phi_4^{POCs}\,sh\cdot POC_b\cdot POC_s
\end{aligned} \tag{1}$$

This parameterisation is based on Jackson (1990) and Kriest and Evans (1999, 2000). The shear rate (sh) is set to 1 $s^{-1}$ in the mixed layer and 0.01 $s^{-1}$ below. The coefficients $\phi(\phi_1^{DOC}, \phi_2^{DOC}, \phi_3^{DOC}, \phi_1^{POCs}, \phi_2^{POC}$ for turbulence coagulation; $\phi_3^{POCs}, \phi_4^{POCs}$ for differential settling) were obtained by integrating the standard curvilinear kernels for collisions over the size range of each organic matter pool (Table 1). Flux feeding by mesozooplankton occurs only on big particles.

To account for the reported increase with depth of sinking speed (Berelson, 2002),

the following parameterisation is applied to the sinking speed of $POC_b$ ($w^{POC}$, m/d):

$$w^{POC} = w^{POC}_{\min} + \left(w^{POC}_{\max} - w^{POC}_{\min}\right) \max\left(0, \frac{z - z_m}{2000}\right) \quad (2)$$

where:

$w^{POC}_{\min}$, minimum sinking speed of $POC_b$, 50 m/d;

$w^{POC}_{\max}$, maximum sinking, 200 m/d;

$z_m$ , depth of mixed layer.

The fraction of $POC_s$ sinks at a constant speed of 3 m/d.

### 2.2.2 Parameterization of size spectrum: number and mass of particles, prognostic sinking speed

In comparison to the standard version of PISCES, which distinguishes two particle size classes of POC and allows for the exchange of matter between size classes by aggregation/disaggregation, but prescribes the corresponding sinking speed, we have implemented a more advanced description of particle dynamics based on the work by Kriest and Evans (1999, 2000). This approach models the size distribution of particles of the detrital pool and their mean sinking speed based on the assumption that the particle size spectrum can be fully described by the number and the mass of particles.

Based on in situ observations, McCave (1984) proposed a power law to represent the particle size distribution $p(\theta)$ as a function of particle diameter $\theta$:

$$p(\theta) = \frac{dN}{d\theta} = A\theta^{-\varepsilon} \quad m < \theta < \infty \quad (3)$$

where: d$N$, number concentration of particles in a given size range $\theta$ to $\theta$+d$\theta$.

The total number of particles larger than $m$ follows from the cumulative size as

$$P(m) = A\int_m^\infty \theta^{-\varepsilon} d\theta = A\frac{m^{1-\varepsilon}}{\varepsilon - 1} \quad \text{provided} \quad \varepsilon > 1. \quad (4)$$



Let the mass $C$ of a particle be related to its diameter $\theta$ by $C(\theta) = C\theta^{\zeta}$ and $C_m = Cm^{\zeta}$ be the mass of a single cell. The total mass of particles follows from the cumulative mass distribution $M(\theta)$ as

$$M(m) = AC\int_m^\infty \theta^{\zeta-\varepsilon} d\theta = AC_m \frac{m^{1+\zeta-\varepsilon}}{(\varepsilon - \zeta - 1)} \text{provided} \quad \varepsilon > \zeta + 1. \quad (5)$$

The exponent $\varepsilon$, the shape of the size distribution, is expressed as a function of $N$, the average number of cells in an aggregate

$$N = \frac{M(m)}{P(m)C_m} = \frac{\varepsilon - 1}{\varepsilon - 1 - \zeta} \quad \text{thus} \quad \varepsilon = \frac{(1+\zeta)N - 1}{N - 1} \quad (6)$$

Sinking modifies the number and the mass of particles in a given parcel of water. The sinking flux of numbers and mass are

$$\phi(z) = \int_m^\infty p(z, \theta)\, \varpi(\theta)\, d\theta \quad \text{, respectively} \quad (7)$$

$$\psi(z) = C\int_m^\infty p(z, \theta)\, \theta^{\zeta}\, \varpi(\theta)\, d\theta \quad (8)$$

where $\varpi(\theta) = B\theta^{\eta}$ is the sinking speed of a particle of size $\theta$.

Aggregation changes the size spectrum, but does not affect particle mass. As in the PISCES standard version, aggregation results from turbulent shear and differential settling. The equation for the rate of collision between particles is (Kriest and Evans, 1999)

$$\xi = 0.5\text{stick}\int_m^\infty \int_m^\infty \left(\beta_{\text{shear}}(\theta, \Theta) + \beta_{\text{sett}}(\theta, \Theta)\right) p(\theta)\, p(\Theta)\, d\theta d\Theta \quad (9)$$

where: stick, non-dimensional parameter of particle stickiness;

$\beta(\theta, \Theta)$ , collision kernel for turbulent (shear) and differential settling (sett);

$p(\theta)$, $p(\Theta)$, particle number distributions.

The stickiness corresponds to the probability of two particles to stick together after collision. The solution of equations 7 to 9 over the finite size spectrum used in this study and their implementation in a vertically resolved model follow Kriest and Evans (2000). Parameter values are summarized in Table 2.

Biological processes like grazing and mortality add to the pool of particles (POC) and modify the mass and size distributions. For instance, flux feeding by mesozooplankton modifies the particle size spectrum by the transfer of mass from big to small particles. Each of the four plankton types encompasses a variety of species and thus a size spectrum. To account for the contribution of the four living compartments to the particle number distribution, we calculated the average size of each pool and its individual cell number equivalent (Table 1). For particles bigger than the single cell, but that are no aggregates, the contribution to $P(m)$ is less than that of aggregates of the same size.

As mentioned above, the dynamic particle mass and number distributions describe the evolution of the detrital pool (POC). The remaining two classes of particles biogenic silica and carbonate are described as in the standard version. Their sinking speed is however no longer imposed. In this version, the hard shell parts sink with the same velocity as computed for the detrital pool.

#### 2.2.3 Mineral ballast model: no information on particle size, prognostic sinking speed

This model version does not distinguish between particle size classes. The sinking speed is prognostic and follows from the average excess density of the particle pool computed from its mean composition in terms of biogenic silica, carbonate and organic matter. The excess density is given by

$$\rho_{\text{excess}} = \frac{m_{\text{POC}}\,[\text{POC}] + m_{\text{CaCO}_3}\,[\text{CaCO}_3] + m_{\text{BSi}}\,[\text{BSi}]}{m_{\text{POC}}/\rho_{\text{POC}}\,[\text{POC}] + m_{\text{CaCO}_3}/\rho_{\text{CaCO}_3}\,[\text{CaCO}_3] + m_{\text{BSi}}/\rho_{\text{BSi}}\,[\text{BSi}]} - \rho_{\text{SW}} \quad (10)$$

where: $m_{\text{POC}}$, $m_{\text{CaCO}_3}$, $m_{\text{BSi}}$, molecular weight of POC (32.7 g), $CaCO_3$ (100 g) and biogenic



silica (72.8 g);

[POC], [$CaCO_3$], [BSI], molar concentration of POC, $CaCO_3$ and biogenic silica;

$\rho_{\text{POC}}$, $\rho_{\text{CaCO}_3}$, $\rho_{\text{BSi}}$, $\rho_{\text{SWi}}$, density of POC (1.06 g/cm$^3$), $CaCO_3$ (2.71 g/cm$^3$), biogenic silica (2.10 g/cm$^3$) and density of seawater (1.027 g/cm$^3$).

The sinking speed follows from $w_{\text{ballast}} = 3\left(\rho_{\text{excess}}/\rho_{\text{POC}} - \rho_{\text{SW}}\right)$, where the lower limit of sinking speed is set to 3 m/d. All particles sink at the same calculated sinking speed.

## 3 The surface sediments

The fluxes of $POC_s$, $POC_b$, BSi and $CaCO_3$ reaching the sediment-water interface are incorporated to the bioturbated sediment layer and undergo early diagenesis as described by Heinze et al. (1999). Within the sediment compartment the two size classes of POC are no longer distinguished. In the original model by Heinze et al. (1999), POC is mineralized solely by oxygen reduction. We added denitrification to the set of early diagenetic reactions. In the model set-up selected for this study, the sediment compartment is not coupled interactively to the water column, but run in an off-line mode. Parameter values are as in Heinze et al. (1999).

## 4 Methodology

### 4.1 Set-up of model experiments

The 3-D global ocean general circulation model OPA (Madec et al., 1998) provided the physical forcing fields for tracer transport. After 3000 years of integration, PISCES reached a quasi steady-state with a mean state and seasonal variations similar to those observed for nutrients and chlorophyll (Aumont and Bopp, 2006). This reference state obtained with the standard version (STD1, two particle size classes, prescribed sinking

speed) was the starting point for 5 model experiments. For each experiment the model was integrated over 100 years. A second set of experiments addressed the sensitivity of mid- and deep-water water fluxes to the aggregation (STD2) and the parameterization of zooplankton feeding (STD3) while keeping the configuration of the standard version. Experiment 4 corresponds to the full aggregation/disaggregation model (K&E, particle size spectrum, prognostic sinking speed), while experiment 5 represents the mineral ballast parameterization (BAL, no information on particle size, prognostic sinking speed). For each of the 5 scenarios, yearly mean fluxes of POC, BSi, $CaCO_3$ and clay were used together with yearly averaged bottom water compositions to equilibrate the surface sediments in an off-line mode. After 50 ky of integration stable distributions of solid and dissolved sediment tracers were obtained.

### 4.2 Model evaluation

The biogeochemical model PISCES was tested over different time ranges and in varying studies: paleoclimatology (Bopp et al., 2003), iron fertilization experiments (Aumont and Bopp, 2006), climate change (Bopp et al., 2005). For this study we selected remote sensing data (SeaWIFS, average surface chlorophyll in mg/m3 over 1997–2004), estimates of export production (Schlitzer 2000 ; Laws et al., 2000), sediment trap POC fluxes (refer to Fig. 2 for location and depth of sediment traps; data are available under http://www.pangea.de, Dittert et al., 2005), surface sediment bulk composition (% dry weight $CaCO_3$, $SiO_2$, Corg from http://www.pangea.de, Dittert et al., 2005) and oxygen fluxes at the sediment-water interface (Jahnke, 1996) for model evaluation. Sediment trap data were not Th-corrected. We selected only data from traps deployed over at least a year and at depths greater than 1000 m, but at least 500 m above the seafloor. While the trapping efficiency of traps deployed in the mesopelagic zone is in general lower than 1, the corresponding efficiency fluctuates around 1 in the bathypelagos (depth>1200 m) (Yu et al., 2001).



## 5 Results and discussion

Model results are presented and compared to data on Figs. 1 to 5: chlorophyll distributions for May and November (Fig. 1), POC export fluxes at 100 m (Fig. 2), POC fluxes across the water column (Fig. 3), surface sediment bulk composition (Fig. 4) and benthic O2 fluxes (Fig. 5). Table 3 summarizes global numbers (primary production, export fluxes, etc.) for each model scenario and presents available independent estimates. These bulk numbers allow a first evaluation of model performance. A detailed discussion of individual model scenarios follows later.

While model derived annual primary production for PISCES-K&E (37 GT C/yr) and PISCES-STD3 (43 GT C/yr) compare favorable to the remote sensing based estimate of 48 GT C/yr, the other model versions yield significantly lower values. Global carbonate production in the model ranges between 0.4 to 1.1 GT C/yr. It falls within the range of published estimates. In the model, between 26 to 29% of the carbonate production is exported at 100 m. The low export flux results from the prescribed routing of carbonate production, where half of the potential production is routed to the sinking particles. Grazing further reduces the sinking carbonate flux by imposing that 50% of grazed shells will dissolve. This description was adopted in order to account for the observed, yet largely unexplained, loss of carbonate production in the upper ocean (Milliman et al., 1999). The model predicts global deposition, as well as burial fluxes of $CaCO_3$ in line with published estimates. Fluxes of BSi derived by PISCES correspond (export fluxes), respectively are slightly greater (depositional and burial fluxes) than published in Tréguer et al. (1995). To conclude, the PISCES model predicts global fluxes that are within the range of uncertainty of published estimates (e.g. Iglesias-Rodriguez et al., 2002; Heinze et al., 2003).

## 5.1 Standard version

## 5.2 Reference run (STD1)

The biogeochemical model PISCES in its standard version reproduces to a large degree the observed large-scale distributions of chlorophyll (Fig. 1), nutrient fields and major phytoplankton groups (Bopp et al., 2005; Aumont and Bopp, 2006). The model overestimates the area of the oligotrophic gyres. In particular in the Northern hemisphere, the transition between the oligotrophic regions and the productive latitudes has a North-South and West-East trend not present in the remote sensing data. This trend in biogeochemical tracer distribution reflects the characteristics of the hydrodynamic forcing fields provided by the model OPA (Madec et al., 1998). Figure 2a compares zonal mean particulate organic C export at 100 m estimated by the model to independent estimates by Schlitzer (2000) and Laws et al. (2000). The PISCES model predicts latitudinal bands of high export fluxes centered at 60° N, 60° S and the Equator. It does neither reproduce the higher and sharper maximum predicted by the inverse model (Schlitzer, 2000), nor its bimodal maximum centered at the Equator. The model predicts lower export fluxes compared to the estimates by Schlitzer (2000). Export fluxes by Laws et al. (2000) show a different zonal pattern with a sharp maximum centered around 40° S, no increased export in the equatorial region and a large export flux in northern high latitudes. This comparison underlines the difficulty in getting reliable estimates of C export out of the euphotic ocean and the necessity for extending the data-model-comparison to other data sets such as sediment trap and surface sediment composition.

The comparison between sediment trap data and model derived POC fluxes is displayed on Fig. 3a. The model predicts a wider spread in POC fluxes between 1000 and 2000 m than present in the data set with a tendency towards overestimation. Modeled deep water fluxes are of the right order of magnitude. Their variability below 3800 m is underestimated by the model.

Material fluxes are integrated to surface sediments, where the oxidation of organic



C is the major driving force of early diagenetic reactions. In the model experiment, the sediment composition was obtained by forcing the sediment with yearly averaged particle fluxes and bottom water concentrations. The resulting distributions of BSi, $CaCO_3$ and TOC (=total organic C) are compared to observations in Fig. 4. Model results are averaged over the bioturbated layer (10 cm). Although the continental margins are included on the Figures, they are not considered in the discussion, since the model does not fully resolve the dominant physical and biogeochemical processes of continental margins. This is reflected by the unrealistic high levels of TOC (Fig. 4a) computed for continental margin sediments. Modeled and measured TOC levels agree in open ocean settings. Similarly, calculated and observed levels of BSi and $CaCO_3$ agree. The modeled distribution of $CaCO_3$ reflects the effect of bathymetry on $CaCO_3$ preservation with high values along topographic heights (e.g. the Mid Ocean Ridge in the Atlantic basin). The BSi content of surface sediments reflects surface ocean diatom productivity: e.g. high values in the Pacific Equatorial upwelling region, low values in the oligotrophic gyres, BSi-rich belt centered at 60° South.

The benthic $O_2$ fluxes provide an integrated measurement of the metabolic activity of surface sediments. Figure 5 presents the comparison between the data based estimate by Jahnke (1996) and model output (Fig. 5b for STD1). While PISCES STD1 reproduces the spatial distribution of $O_2$ fluxes, it underestimates its absolute value in sediments overlain by productive waters.

The mean sinking speed of POC is plotted against depth in Fig. 6. Below the mixed layer, it results from the relative contribution of small and large particles to total POC flux. The sinking speed increases with depth up to 200 m/d. Such high sinking speeds have been reported for marine snow (Alldrege and Gotschalk, 1988) and zooplankton faecal pellets

## 5.3 Aggregation-disaggregation (STD2)

The chlorophyll distributions (Fig. 1), export fluxes (Fig. 2a), POC fluxes across the water column (Fig. 3a) and benthic O2 fluxes (Fig. 5c) predicted by PISCES STD2 are

strikingly similar to the reference version STD1. The same holds for the mean sinking speed (Fig. 6). Both model versions differ with respect to aggregation-disaggregation which is not represented in STD2. The lack of differences between both versions suggests that processes of aggregation and disaggregation are only of second order importance in controlling yearly averaged fluxes of POC across the water column in the standard model formulation.

#### 5.3.1 Flux feeding intensity (STD3)

From the preceding follows, that the model in its standard version (STD1) predicts export fluxes of POC out of the euphotic zone lower than those by Schlitzer (2000), while particle fluxes across the water column and down to the sediment water interface are well represented. The majority of POC exported from the euphotic ocean is mineralized in the mesopelagos by the combined activity of bacteria and zooplankton. Among zooplankton, flux feeding mesozooplankton appears to be the main responsible agent of flux reduction (Stemman et al., 2004b). These organisms feed preferentially on fast falling particles (Jackson, 1993) and the feeding intensity scales with flux rather than with concentration. The preference for fast falling particles is transposed to the model by limiting flux feeding ($g^{meso}$) to POCb. The corresponding parameterization reads

$$g^{meso}(\mathrm{POCb}) = g^{meso}_{FF} w^{\mathrm{POCb}} \frac{\mathrm{POCb}}{K^{FF}_{\mathrm{POCb}} + POCb}, \quad (11)$$

where

$g^{meso}_{FF}$, maximum rate of flux feeding, 1/m

$K^{FF}_{\mathrm{POCb}}$, half saturation constant for flux feeding, $\mu$mol C/l

$w^{\mathrm{POCb}}$, sinking velocity of POCb, m/d.

Flux feeding does not increase infinitively with flux. This behaviour is accounted for by a Michaelis-Menten type function. To test the sensitivity of the model parameterization to the intensity of flux feeding, we did a second experiment multiplying the



maximum flux feeding rate $g^{meso}_{FF}$ by a factor two ($g^{meso}_{FF}$=3.5 $10^{-4}$ in STD1; $g^{meso}_{FF}$=7.0 $10^{-4}$ in STD3).

Increasing the intensity of flux feeding slightly improves the large scale distributions of surface ocean biological tracers as exemplified for chlorophyll fields in Fig. 1. Modeled chlorophyll concentrations in the oligotrophic gyres are higher and closer to satellite derived estimates, which translates into an increase in primary production from 26 GT C/yr in PISCES-STD1 to 43 R GT C/yr in PISCES-STD3. The higher productivity is also reflected by increased export fluxes in the oligotrophic gyres and at the Equator (Fig. 2a). PISCES-STD3 predicts export fluxes of similar magnitude than Schlitzer (2000) in these latitudinal bands. Modeled POC fluxes correspond to trap data (Fig. 3c) over the 1000 to 2000 m depth range. Deep water fluxes are, however, largely underestimated by the model with values below 10 mmolC/m$^2$/yr. The starving of the bathypelagos is further emphasized by the comparison of predicted $O_2$ fluxes at the sediment-water interface (Fig. 5d). Neither the spatial pattern nor the intensity of $O_2$ fluxes present in the large scale distribution of Jahnke (1996) is reproduced by PISCES-STD3.

Increasing flux feeding intensity in PISCES-STD3 deteriorates the representation of deepwater POC fluxes. Flux feeding impacts the flux of big POC particles. Increasing flux feeding in the model standard version, decreases the flux of fast sinking POCb and thereby lowers the average sinking speed (Fig. 6). It translates into a more intense POC recycling in the mesopelagos and thus an overall shallower penetration of POC in the water column. This fuels the productivity at the boundary, as well as in the oligotrophic gyres, giving rise in turn to higher POC export at 100 m. Particle fluxes are very sensitive to the process of flux feeding. In line with our results, Stemman et al. (2004a, b) emphasize the importance of flux feeding in a 1-D model study of particle fluxes at the Mediterranean time series station Dyfamed.

## 6 Full size spectrum and mineral ballast model

The capability of the model versions PISCES-K&E and PISCES-BAL to reproduce surface ocean biological tracer distributions is exemplified for spring and fall chlorophyll distributions. Figure 1 compares model output of the full size spectrum model (K&E) and of the mineral ballast model (BAL) to Seawifs data. The tendency to overestimate the aerial extension of oligotrophic gyres is also found in the model versions PISCES-K&E and PISCES-BAL. Predicted global rates of yearly primary production range at the lower (PISCES-BAL), respectively higher (PISCES-K&E) end of model estimates. The inverse is obtained for POC export at 100 m: PISCES-K&E yields the lowest and PISCES-BAL the highest POC export (Fig. 2b) of all simulations. The mineral ballasting parameterization predicts highest export fluxes in areas where the model computes a high contribution of diatoms (e.g. centered at 60° S), respectively calcareous nanophytoplankton (e.g. centered at 40° S) to primary production.

The evolution with depth of sinking speed (Fig. 6) in PISCES-K&E reveals values below 3 m/d down to 50 m, followed by a rapid increase up to 50 m/d between 50 and 500 m. The strong increase in sinking speed occurs to the base of the mixed layer where high concentration of particles and high turbulence promote particle coagulation. The overall low sinking speed computed over the upper 100 m contributes to the low export production predicted by PISCES-K&E (Fig. 2b). Low sinking speeds imply longer particle residence times at shallow depth, shallower remineralization and in turn less POC export. This is further emphasized by Fig. 7 representing mean POC fluxes as a function of depth for PISCES-STD1, PISCES-K&E and PISCES-BAL. Particulate organic C fluxes peak around 100 m (Fig. 7). The decrease with depth is less pronounced in PISCES-K&E: 46% of the POC flux predicted at 100 m survives to 1000 m, as compared to 34% in the reference version PISCES-STD1 or in PISCES-BAL. High POC fluxes prevail down to sediment in the case of the ballast parameterization.

The comparison between modeled POC fluxes and our data base, suggests that updating the standard version of PISCES to take into account the particle size spec-



trum and a prognostic sinking speed (PISCES-K&E, Fig. 3d) does not significantly improve the fit of model output to data compared to the reference version PISCES-STD1 (Fig. 3a). Modeled benthic O2 fluxes (Fig. 5e) agree in terms of large scale distribution and order of magnitude with the independent estimate by Jahnke (1996).

The correspondence between modeled POC fluxes and trap data is slightly improved in PISCES-BAL (Fig. 3e). Similar to model versions PISCES-STD1 and PISCES-K&E, the model overestimates fluxes between 1000 and 2000 m. They are of the right order of magnitude below 2000 m. The model predicts benthic O2 fluxes (Fig. 5e) of a large scale distribution similar to the one published by Jahnke (1996). However southern latitudinal gradient across areas of low and high O2 fluxes is too strong in the model results. This suggests that in areas of high diatom and calcareous nanophytoplankton productivity, the model overestimates deep water POC fluxes.

The tendency of the model to overestimate POC fluxes between roughly 1000 and 2000 m is present in all model versions, but PISCES-STD3. An evaluation of trapping efficiency of sediment traps (Yu et al., 2001) suggests a low and erratic efficiency in the mesopelagic. This is also confirmed by a comparison between sediment trap data and inverse modeling results (Usbeck et al., 2003). The low trapping efficiency of sediment traps at mid-depth might explain the systematic off-set between modeled fluxes and trap results.

## 7 Conclusions

This paper highlights the difficulties in reconciling surface ocean observations, mid- to deep-water particle fluxes and sediment data. The comparison of three descriptions of particle dynamics of differing complexities allows a first appreciation of the processes that have to be included in order to achieve a correct representation of pelagic-benthic coupling at the global ocean scale. Predicted POC fluxes in the mesopelagos are most sensitive to the intensity of zooplankton flux feeding. An improved description of this feeding type calls for an extended set of experimental data. All model parameters

being kept constant and for a given intensity of flux feeding, the capability of the model to reproduce yearly averaged POC fluxes and benthic oxygen demand does in first order not dependent on the resolution of the particle size spectrum. Model results obtained with the PISCES standard version PISCES-STD1 (2 particle size classes and sinking speed prescribed for each size class) and with PISCES-K&E (particle size spectrum and prognostic sinking speed) are similar. The model version that predicts the sinking speed from the effect of ballasting of POC fluxes by minerals and thus ignoring particle size, gives the best fit between modeled and observed POC fluxes below 2000 m and down to the sediment-water interface. While our model study does not allow to conclusively identify whether particle aggregation or mineral ballasting is the key mechanism controlling POC fluxes in the ocean interior (Passow, 2004), it suggests that aggregate formation alone might not be sufficient to drive an intense biological pump. High particle fluxes down to the bathypelagos are most likely the result of the combined effect of aggregate formation and mineral ballasting (Passow and DeLaRocha, 2006).



*Acknowledgements.* This work was supported through grants EVK2-CT-2001-00100 (EU FP5 RTD project ORFOIS), GOCE-511176 (EU FP6 IP CarboOcean) by the European Commission and by the French national program PROOF/OCEVAR. This LSCE publication number XX.

## References

Alldredge, A. L. and Gotschalk, G.: In situ settling behaviour of marine snow, Limnol. Oceanogr., 33, 339–351,1988.

Armstrong, R. A., Lee, C., Hedges, J. I., Honjo, S., and Wakeham, S. G.: A new, mechanistic model for organic carbon fluxes in the ocean based on the quantitative association of POC with ballast minerals, Deep Sea Res. I, 49, 219–236, 2002.

Aumont, O., Maier-Reimer, E., Monfray, P., Blain, S., and Pondaven, P.: An ecosystem model of the global ocean including Fe, Si, P co-limitations, Global Biogeochem. Cycles, 17(2), 1060, doi:10.1029/2001GB001745, 2003.

Aumont, O. and Bopp, L.: Globalizing results from ocean in situ iron fertilization studies, Global Biogeochem. Cycles, 20(2), 2017, doi:10.1029/2005GB002591, 2006.

Berelson, W. M.:. Particle settling rates increase with depth in the ocean, Deep Sea Res. II, 49, 237–251, 2002.

Berner, R. A.: A model for atmospheric $CO_2$ over Phanerozoic time, Am. Jour Sci., 291, 339–376, 1991.

Betzer, P. R., Showers, W. J., Laws, E. A., Winn, C. D., DiTullio, G. R. and Kroopnick, P. M.: Primary productivity and particle fluxes on a transect of the equator at 153° W in the Pacific Ocean, Deep Sea Res., 31, 1–11. 1984.

Bopp, L., Kohfeld, K. E., Le Quéré, C., and Aumont, O.: Dust impact on marine biota and atmospheric $CO_2$ during glacial periods, Paleoceanogr., 18, 1046, doi:10.1029/2002PA000810, 2003.

Bopp, L., Aumont, O., Cadule, P., Alvain, S., and Gehlen, M.: Response of diatoms distribution to global warming and potential implications: A global model study, Geophys. Res. Lett., 32, L19606, doi:10.1029/2005GL023653, 2005.

Dittert, N., Corrin, L., Bakker, D., Bendtsen, J., Gehlen, M., Heinze, C., Maier-Reimer, E., Michalopoulos, P., Soetaert, K. E. R., and Tol, R. J. S.: Integrated Data Sets of the FP5 Research Project ORFOIS: Origin and fate of biogenic particle fluxes in the ocean and their

interactions with atmospheric $CO_2$ concentrations as well as the amrine sediment (Vol. 1), WDC-MARE Reports 0002, 2005.

Volk, T. and Hoffert, M. I.: Ocean carbon pumps, analysis of relative strengths and efficiencies in ocean-driven atmosphere $CO_2$ changes, in: The Carbon Cycle and Atmospheric $CO_2$: Natural Variations Archean to Present, edited by: Sundquist, E. T. and Broecker, W. S., Geophys. Monogr., AGU, Washington, D.C., 32, 99–110, 1985.

François, R., Honjo, S., Krishfield, R., and Manganini, S.: Factors controlling the flux of organic carbon to the bathypelagic zone of the ocean, Global Biogeochem. Cycles, 16, doi:10.1029/2001GB001722, 2002.

Heinze, C., Maier-Reimer, E., Winguth, A. M. E., and Archer, D.: A global oceanic sediment model for long-term climate studies, Global Biogeochem. Cycles, 13, 221–250, 1999.

Heinze, C., Hupe, A., Maier-Reimer, E., Dittert, N., and Ragueneau, O.: Sensitivity of the marine biospheric Si cycle for biogeochemical parameter variations, Global Biogeochem. Cycles, 17, 1086, doi:10.1029/2002GB001943, 2003.

Iglesias-Rodriguez, M. D., Armstrong, R., Feely, R., Hood, R. Kleypas, J., Milliman, J. D., Sabine, C., and Sarmiento, J.,: Progress made in study of ocean's calcium carbonate budget, Eos Trans. AGU, 83, 365, 2002.

Jackson, G. A.,: A model for the formation of marine algal flocs by physical coagulation processes, Deep Sea Res., 37, 1197–1211, 1990.

Jackson, G. A.: Flux feeding as a mechanism for zooplankton grazing and its implications for vertical particulate flux. Limnol. and Oceanogr., 38, 1328–1331, 1993.

Jahnke, R. A.: The global flux of particulate organic carbon : Areal distribution and magnitude, Global Biogeochem. Cycles, 10, 71–88, 1996.

Klaas, C. and Archer, D. E.: Association of sinking organic matter with various types of mineral ballast in the deep sea: Implications for the rain ratio, Global Biogeochem. Cycles, 16, 116, doi:10.1029/2001GB001765, 2002.

Kriest, I. and Evans, G. T.: Representing phytoplankton aggregates in biogeochemical models, Deep Sea Res. I, 46: 1841–1859, 1999.

Kriest, I. and Evans, G. T.: A vertically resolved model for phytoplankton aggregation., Proc. Indian Acad. Sci. Earth Planet. Sci., 109, 453–469, 2000.

Laws, E. A., Falkowski, P. G., Smith Jr., W. O., Ducklow, H., and McCarthy, J. J.: Temperature effects on export production in the open ocean, Global Biogeochem. Cycles 14(4): 1231–1246, 2000.



Le Quéré, C., Harrison, S. P., Prentice, I. C., Buitenhuis, E. T., Aumont, O., Bopp, L., Claustre, H., Da Cunha, L. C., Geider, R., Giraud, C., Klaas, C., Kohfeld, K. E., Legendre, L., Manizza, M., Platt, T., Rivkin, R. B., Sathyendranath, S., Uitz, J., Watson, A. J., and Wolf-Gladow, D.: Ecosystem dynamics based on plankton functional types for global ocean biogeochemistry models, Glob. Change Biol., 11(11), 2016–2040, 2005.

Madec, G., Delecluse, P., Imbard, M., and Lévy, C.: OPA8.1 Ocean general circulation model reference manual, Notes du pôle de modélisation, IPSL, 1998.

Martin, J. H., Knauer, G. A., Karl, D. M., and Broenkow, W. W.: VERTEX: carbon cycling in the northeast Pacific, Deep Sea Res., 34, 267–285, 1987.

McCave, I. N.: Size spectra and aggregation of suspended particles in the deep ocean, Deep-Sea Res., 31(4), 329–352, 1984.

Milliman, J. D. and Droxler, A. W.: Neritic and pelagic carbonate sedimentation in the marine environment: ignorance is not bliss, Geologische Rundschau 85, 496–504, 1996.

Milliman, J. D., Troy, P. J., Balch, W. M., Adams, A. K., Li, Y.-H., and Mackenzie, F. T.: Biologically mediated dissolution of calcium carbonate above the chemical lysocline, Deep Sea Res. I, 46, 1653–1669, 1999.

Moore, K. J., Doney, S. C., and Lindsay, K.: Upper ocean ecosystem dynamics and iron cycling in a global three-dimensional model, Global Biogeochem. Cycles, 18, doi:10.1029/2004GB002220, 2004.

Passow, U.: Switching perspectives: Do mineral fluxes determine particulate organic carbon fluxes or vice versa?, Geochem. Geophys. Geosyst., 5, doi:10.1029/2003GC000670, 2004.

Passow, U. and De La Rocha, C. L.: Accumulation of mineral ballast on organic aggregates, Global Biogeochem. Cycles, 20, doi:10.1029/2005GB002579, 2006.

Schlitzer, R.: Applying the adjoint method for biogeochemical modeling: Export of particulate organic matter in the World Ocean. Inverse methods in: biogeochemical cycles, P. Kasibhata, AGU Monograph, 114, 107–124, 2000.

Stemmann, L., Jackson, G. A., and Ianson, D.: A vertical model of particle size distributions and fluxes in the midwater column that includes biological and physical processes – Part I: model formulation, Deep Sea Res. I, 51, 865–884, 2004.

Stemmann, L., Jackson, G. A., and Gorsky, G.: A vertical model of particle size distributions and fluxes in the midwater column that includes biological and physical processes – Part II: application to a three year survey in the NW Mediterranean Sea, Deep Sea Res. I, 51, 885–908, 2004.

Suess, E.: Particulate organic carbon flux in the oceans – Surface productivity and oxygen utilization, Nature 288, 258–263, 1980.

Tréguer, P.: Silica and the cycle of carbon in the ocean, C. R. Geoscience, 334, 3–11, 2002.

Turner, J. T.: Zooplankton feacal pellets, marine snow and sinking phytoplankton blooms, Aquatic Microbial Ecology, 27, 57–102, 2002.

Usbeck, R., Schlitzer, R., Fischer, G., and Wefer, G.: Particle fluxes in the ocean: Comparison of sediment trap data with results from inverse modeling, Jour. Mar. Sci., 39, 167–183, 2003.

Wassmann, P., Hansen, L., Andreassen, I. J., Riser, C. W., and Urban-Rich, J.: Distribution and sedimentation of faecal pellets on the Nordvestbanken shelf, northern Norway, in 1994, Sarsai, 84, 689–692, 1999.

Yu, E.-F., François, R., Bacon, M. P., Honjo, S., Fleer, A. P., Manganini, S. J., Rutgers van der Loeff, M. M., and Ittekot, V.: Trapping efficiency of bottom-tethered sediment traps estimated from the intercepted fluxes of 230 Th and 231 Pa, Deep Sea Res. I, 48, 865–889, 2001.



**Table 1.** Size range of particle classes identified in the model and corresponding average size. The number equivalent of size class in terms of single cells.

| Particle type | size range($\mu$m) | average size($\mu$m) | number equivalent |
|---|---|---|---|
| nanophytoplankton | 2–20 | 6.32 | 2.3 |
| diatoms, microzooplankton | 10–200 | 45 | 3.7 |
| mesozooplankton | 200–2000 | 632 | 7.0 |
| aggregate | 200–5000 | 1000 | 9.9 |

**Table 2.** Parameter values of PISCES-K&E.

| Parameter | units | PISCES K&E |
|---|---|---|
| sinking exponent($\eta$) | dimensionless | 1.17 |
| sinking factor (B) | dimensionless | 942 |
| particle mass–diameter exponent($\zeta$) | dimensionless | 2.28 |
| Stickiness | dimensionless | 0.5 |
| mass of single cell | g | 0.0002 |
| upper limit of aggregate mass | g | 1.0 |
| shear (mixed layer) | 1/s | 1.0 |
| shear (below mixed layer) | 1/s | 0.01 |



**Table 3.** Comparison between global fluxes predicted by the different model versions and independent estimates. Units are in GT carbon (POC and $CaCO_3$) or silicon (BSi) per year.

| Model | STD1 | STD2 | STD 3 | K& E | Ballast | Ind. Est. |
|---|---|---|---|---|---|---|
| Global production rates (GT C or Si per yr) | | | | | | |
| PP | 26 | 28 | 43 | 37 | 21 | 48[(1)] |
| BSi | 5.0 | 5.0 | 5.0 | 5.0 | 6.0 | 6.7[(3)] |
| $CaCO_3$ | 0.7 | 0.8 | 1.2 | 1.1 | 0.4 | 0.72–1.4[(2)] |
| Global export rates at 100 m (GT C or Si per yr) | | | | | | |
| POC | 8.0 | 8.0 | 10 | 5.0 | 11 | |
| BSi | 4.0 | 4.0 | 4.0 | 4.0 | 4.0 | 3.4[(3)] |
| $CaCO_3$ | 0.2 | 0.2 | 0.3 | 0.3 | 0.1 | |
| Flux at sediment-water interface below 1000 m (GT C or Si per yr) | | | | | | |
| POC | 0.4 | 0.4 | 0.1 | 0.5 | 0.9 | |
| BSi | 3.0 | 3.0 | 3.0 | 3.0 | 2.0 | 0.8[(3)] |
| $CaCO_3$ | 0.2 | 0.2 | 0.3 | 0.3 | 0.1 | 0.3[(4)] |
| Global burial fluxes below 1000 m (GT C or Si per yr) | | | | | | |
| POC | 0.17 | 0.17 | 0.08 | 0.19 | 0.40 | 0.04[(5)] |
| BSi | 0.40 | 0.42 | 0.33 | 0.41 | 0.12 | 0.17[(3)] |
| $CaCO_3$ | 0.04 | 0.04 | 0.07 | 0.06 | 0.02 | 0.10[(2)] |

[(1)] Vertically Generalized Production Model (VGPM) – http://marine.rutgers.edu/opp/; [(2)] Iglesias–Rodriguez et al. (2002); [(3)] Tréguer (2002); [(4)] flux at 1000 m after Milliman and Droxler (1996); [(5)] POC burial estimated after Berner (1991) as $C_{POC}$ burial=0.25×$C_{CaCO3}$ burial.

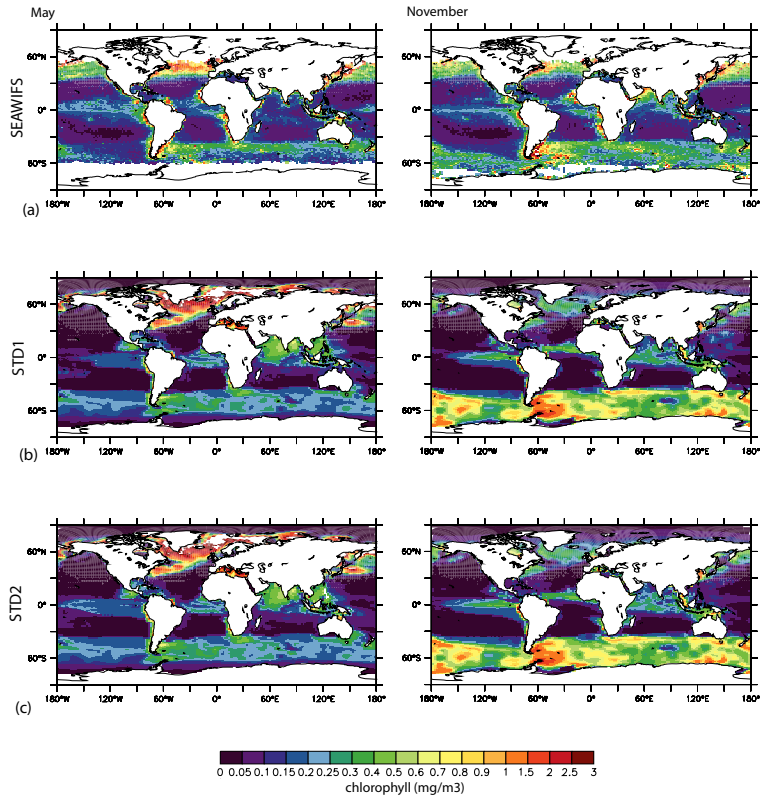


**Fig. 1.** Comparison between mean chlorophyll concentrations (mgChl/$m^3$) for May and November from SeaWifs and model output. **(a)** SeaWifs, **(b)** PISCES-STD1, **(c)** PISCES-STD2, **(d)** PISCES-STD3, **(e)** PISCES-K&E, **(f)** PISCES-BAL.



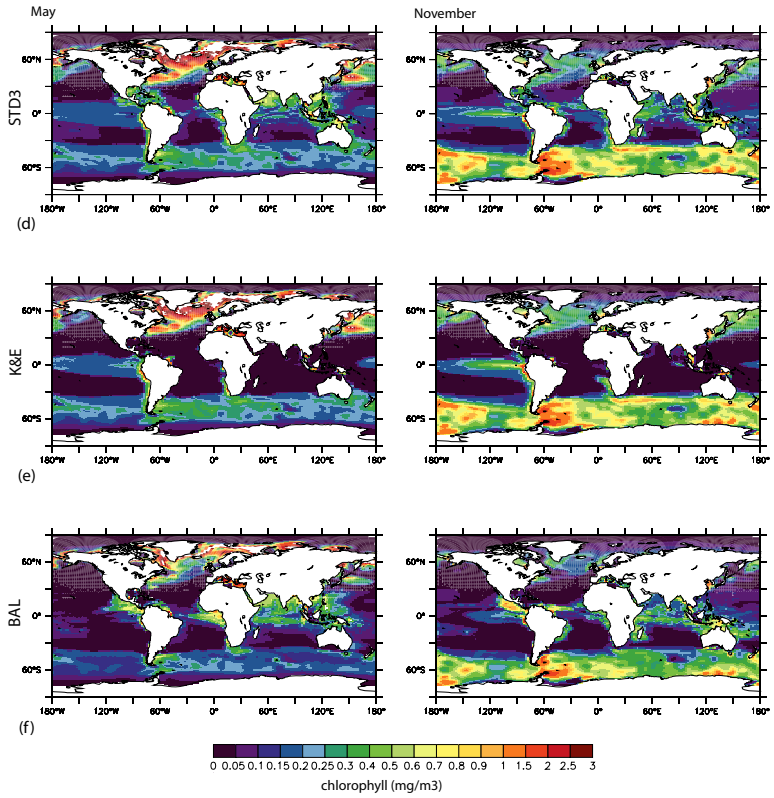


**Fig. 1.** Continued.

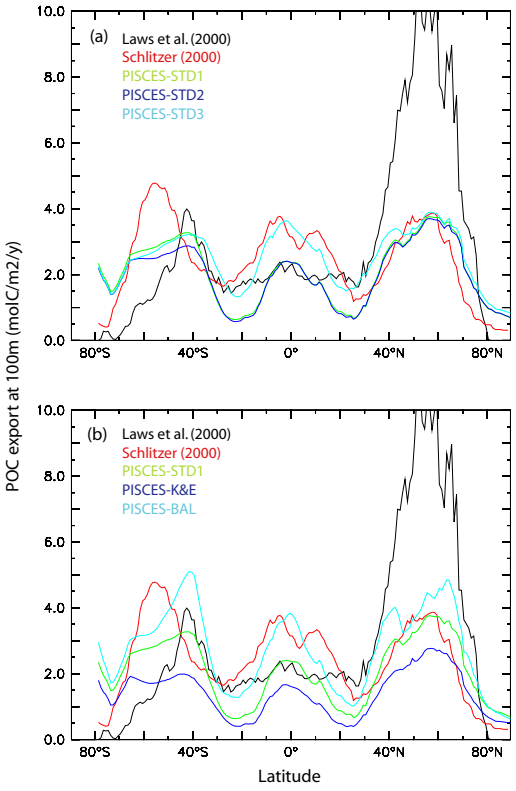


**Fig. 2.** Zonal mean particulate organic carbon export fluxes at 100 m (mol/m$^2$/y). Comparison published estimates and model results: **(a)** PISCES-STD1, PISCES-STD2, PISCES-STD3; **(b)** PISCES-STD1, PISCES-K&E, PISCES-BAL.

831

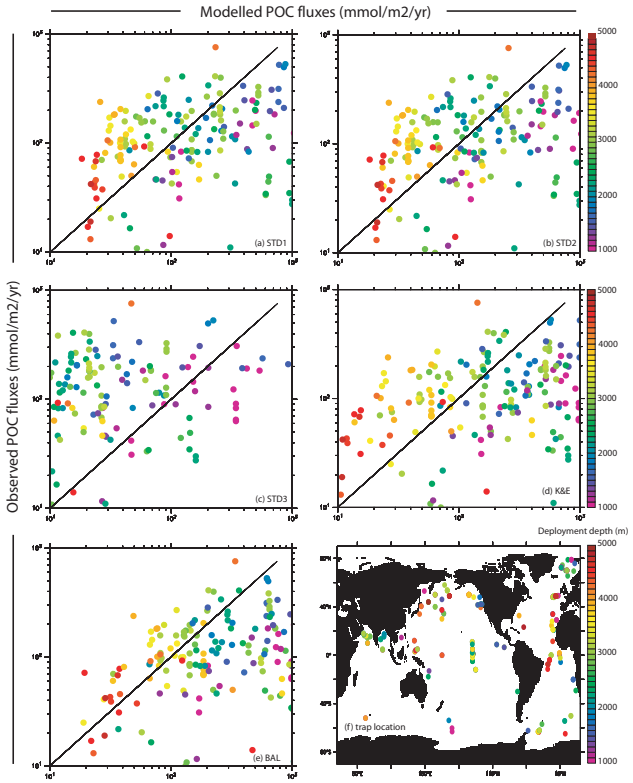


**Fig. 3.** Comparison between POC fluxes (mol C/m$^2$/y) estimated from sediment traps and modeled fluxes. The color code corresponds to the depth of deployment of sediment traps. Values <10 mmol C/m$^2$/y are excluded from the graph.

832

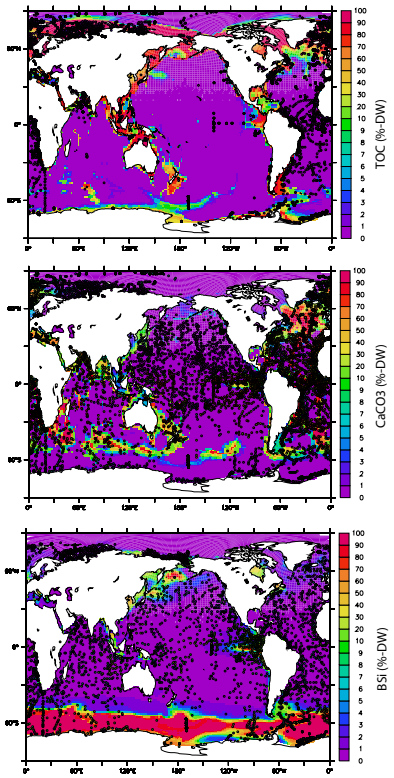


**Fig. 4.** Bulk composition of surface sediments (upper 10 cm). **(a)** POC, **(b)** $CaCO_3$, **(c)** BSi. All expressed in %-dry weight. Data are included as dots on the same colour scale.



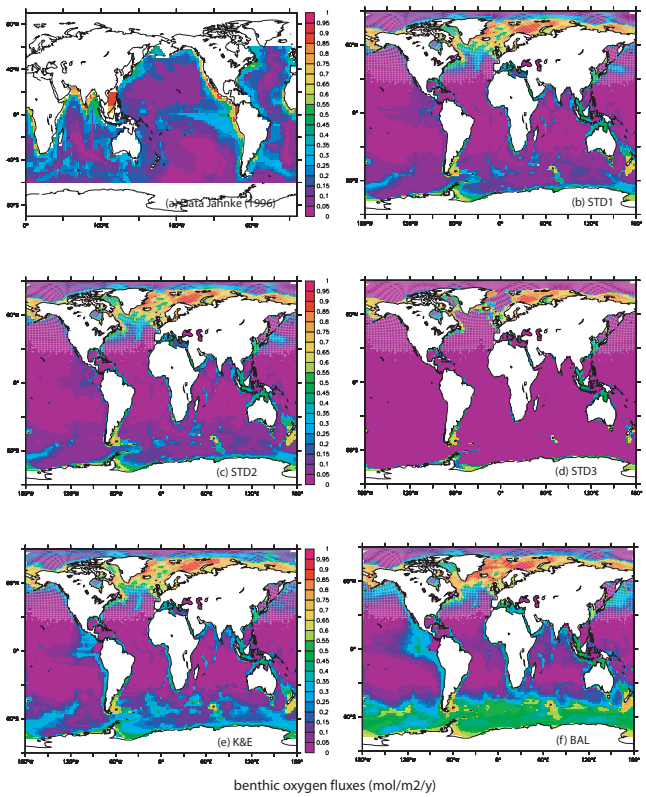


**Fig. 5.** Oxygen fluxes (mol/m2/y) at the sediment water interface: **(a)** independent estimate by Jahnke (1996); predicted by the model. **(b)** PISCES-STD1, **(c)** PISCES-STD2, **(d)** PISCES-STD3, **(e)** PISCES/K&E, **(f)** PISCES/BAL.

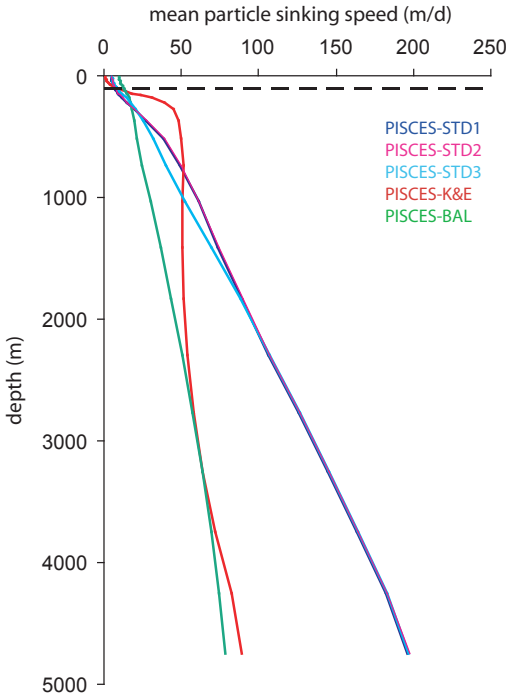


**Fig. 6.** Global mean sinking speed (m/d) as a function of depth of water column predicted by different model versions.



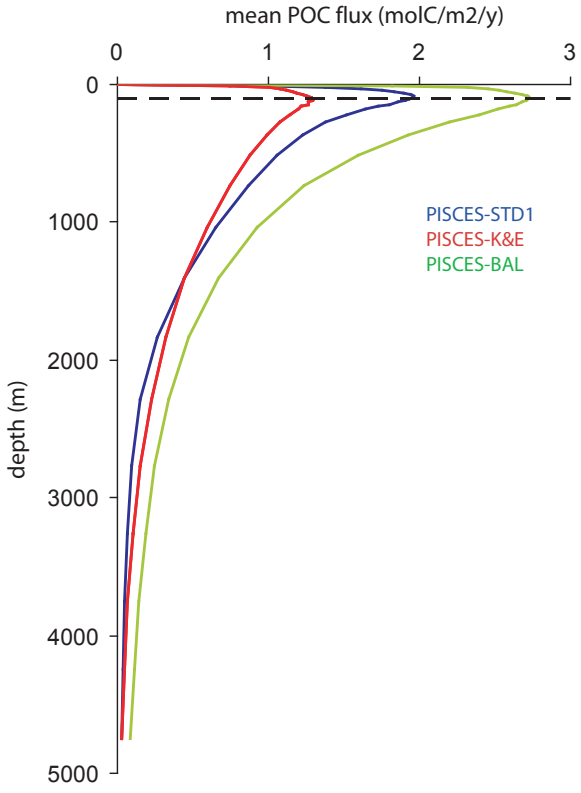


**Fig. 7.** Modelled global mean POC fluxes (m/d) as a function of depth of water column.